Curvature instability in fluid membranes with polymer lipids subject to tension

T. Kohyama
Faculty of Education, Shiga University, Otsu 520, Japan
(Received 20 August 1997)

Shape transformations of a flat fluid membrane with polymer lipids subject to lateral tension are studied as an approximation for multimembrane systems. Using Monte Carlo simulations, we find several characteristic structures of membranes, such as thermal fluctuations, large localized deformations, and undulations due to a curvature instability. The effect of thermal fluctuations on the curvature instability is investigated, and the undulations are characterized by a single-mode approximation for unstable modes. It is shown that thermal fluctuations, the curvature instability and vesiculation determine the parameter region in which an undulating membrane is observed. The phase diagram of undulation obtained through simulations closely resembles that measured experimentally for ''biogels.'' This suggests that the undulation corresponds to defects in multimembrane systems and that the curvature instability is the main cause of defect formation in ''biogels.'' [S1063-651X(98)16105-6]

PACS number(s): 68.10.−m

I. INTRODUCTION

Complex properties of fluid membranes composed of amphiphilic substances have attracted a great deal of attention [1]. Fluid membranes, for example biological membranes, often contain many kinds of polymer inclusions which in many cases affect the physical properties of the membranes, such as elasticity. The effects of polymer inclusions in fluid membranes have been studied extensively, and the interaction between inclusions has been analyzed theoretically [2,3]. The effect of inclusions in multilamellar systems has also been discussed [4]. These membranes with inclusions are important not only theoretically, but also for many applications, including the design of drugs.

Recently, an interesting observation has been made for multilamellar lipid membranes with long polymer lipids in both bilayers, and it was found that the viscoelastic properties of the system change from those of a fluid to those of a gel when the concentration of polymer lipids and the water fraction satisfy a certain condition [5]. The substances in this gel state are called ''biogels'' [5] or ''hydrogels'' [6]. The transition points to the gel state depend on the concentrations of the intercalated polymer lipids in the membranes and the distance between neighboring membranes in the multilamellar phase. Increasing the water fraction under a constant concentration of polymer lipids, the fluid lamellar phase present at low water fraction changes to a gel phase at a critical water fraction. Increasing the water fraction further, the gel phase eventually disappears as a fluid phase reappears. Since a high water fraction implies a large spacing between neighboring membranes, we can say that the system is in the fluid lamellar phase when the spacing is small, and that the gel phase appears when the spacing is in a certain range. When the spacing exceeds this range, the viscoelasticity of the system again becomes fluidlike. A similar behavior is observed when the concentration of polymer lipids is gradually increased from a low value. At low concentrations of polymer lipids, the state is in a fluid lamellar phase, but, upon increasing the concentration, it changes to a gel phase at a critical point and remains in the gel state over a certain range of the polymer lipid concentration. At a higher concentration, the viscosity of the system returns to that of a fluid. By x-ray scattering methods [5], some kinds of defects in the multilamellar phase have been observed. These are thought to play an important role in the gel formation. Recent direct observations employing freeze-fracture electron microscopy [6] have clarified the defect structures. They have revealed many complicated vesicular and cylindrical defects which are connected when the system is in the gel phase.

In a previous work, we theoretically described the phase diagram of the concentration of polymer lipids and the spacing between neighboring membranes, measured by experiments [5]. Assuming that the sizes of defects in the multilamellar phase do not depend strongly on the spacing between neighboring membranes, we roughly determined the defect structures and estimated the volume fractions [7]. In this theory, we assumed that the complicated structures of the defects act as bridges, connecting many membranes, and that the transition from the fluid phase to the gel phase takes place when the regions connected by the defects occupy nearly the entire system, as in the case of percolation phenomena [8]. When the concentration of polymer lipids is too high or the spacing between membranes is too large, the binding force between membranes due to defects decreases, and the defects begin to move as vesicles. In this case, the system is considered as an assembly of vesicles and lamella, and has a fluid viscosity.

Although defect structures in the multilamellar phase play a crucial role in gel formation, three-dimensional structures and size distributions have not been elucidated either experimentally or theoretically. In this paper, we study the shapes of membranes (strings) in two-dimensional space. Such a system can be considered as a two-dimensional slice of a three-dimensional structure. As a first approximation of multilamellar systems, we describe the shape transformation of one lipid membrane (string) with polymer lipids subject to lateral tension. If we assume that neighboring membranes exert repulsive interactions, shape fluctuations in the direction normal to the membrane increase the interaction energy between neighboring membranes. This energy increase can

be interpreted as lateral tension in the membrane. If each membrane fluctuates with weak correlation, and the fluctuation is small compared to the average spacing between neighboring membranes, a one-membrane system with lateral tension is derived as a kind of mean-field approximation. Since neighboring membranes are strongly correlated in some cases, and the shape transformations become large, this one-membrane approximation is not appropriate for these cases, but we believe that the elucidation of the natures of the one-membrane system is an instructive and helpful first step in determining the defect structures in multilamellar systems. Experiments with the one-membrane system applying a tension can be done by controlling osmotic pressure.

One-membrane systems with two order parameters generate a so called ''curvature instability'' [9,10], and in this context lamella and vesicles have been studied extensively [11–13]. In this paper we investigate the effect of lateral tension and the presence of polymer lipids on the shape transformations of flat membranes, using finite-temperature Monte Carlo simulations [14] and an analytic study. We find that when the concentration of polymer lipids is small, only thermal fluctuations of membranes are observed, but, at a certain concentration, a small number of largely deformed parts appear. This appearance is considered as corresponding to defect structures in multilamellar systems. Increasing the concentration further, the locally deformed parts extend, and the membrane exhibits a uniform undulation over the entire area. At a higher concentration, the membrane changes to a flat shape because of the large effective bending coefficient. Under a constant concentration of polymer lipids, the membrane shape is changed by the lateral tension. Decreasing the tension from a large value, the flat membrane changes to exhibit an undulating shape at a certain tension. Further decreasing the tension, some part of the membrane (string) begins to touch other parts of the membrane. In the simulation, this situation is meaningless, but we conjecture that vesicles become stable near this point in multilamellar systems. The phase diagram obtained for the membrane corresponds well to that obtained by experiments on real ''biogels'' [5].

In Sec. II, we define the free energy of a one-lipid membrane with polymer lipids subject to lateral tension. In Sec. III, we discuss the linear stability of the flat membrane and the effect of thermal fluctuations. We derive the parameter regions in which the undulation due to the instability is larger than thermal fluctuations. The results of Monte Carlo simulations are summarized in Sec. IV. We find three characteristic undulating shapes. In order to analyze the undulating membranes, we use a single-mode approximation for undulating membranes and determine the amplitudes of undulations and the wave numbers in Sec. V. We restricted the amplitude so that it would not exceed a certain value, because larger values correspond to the situation in which one part of the membrane contacts another part. Combining this condition and the results obtained in Sec. III, we determine the parameter region in which the undulating membranes are observed. These results are compared with those obtained in the Monte Carlo simulations.

II. MODEL SYSTEM

In this section we define a mathematical model of a one-layer lipid membrane subject to lateral tension in two dimensions to study shape transformations. With this one-layer membrane model, it is not possible to observe the defect structures found in multilamellar systems, but this model is more tractable than a multilamellar model and relatively easily studied in detail. This study is instructive in understanding the phenomena displayed by multilamellar systems. As mentioned below, a membrane with external tension on both ends is a kind of mean-field approximation of multilamellar systems with a repulsive interaction between neighboring membranes, like steric interaction [15–17] of thermally fluctuating membranes. When a repulsive interaction is considered, and there is assumed to be only weak correlation between neighboring undulating membranes, each undulating membrane possesses more energy than would a flat membrane, because the effective distance between neighboring membranes decreases and repulsive force becomes stronger. This excess energy due to the undulation can be regarded as the effective lateral tension exerted on the two ends of the membrane. In general, this effective lateral tension depends on the shape of the membrane, but we assume it to be constant. This mean-field approximation is only appropriate when the amplitude of the undulation is small compared to the average distance of the neighboring membranes. Experimentally, this tension can be realized through manipulation of osmotic pressure.

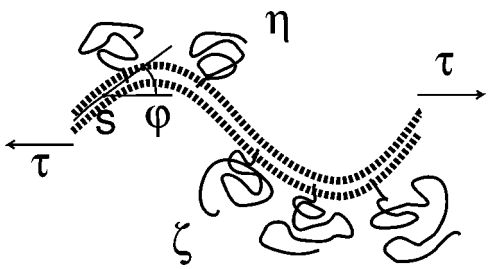

FIG. 1. Schematic representation of the lipid membrane with polymer lipids. The membrane is composed of bilayers, where lipids with long polymers are contained in each layer. The concentrations of polymer lipids in the two layers are denoted by η and ζ. The tension at either end of the membrane is written as τ. The shape of the membrane is described by the tangential angle φ at each position along the membrane, parametrized by s.

As shown in Fig. 1, we consider an incompressible lipid membrane (string) of length L, which experiences a lateral tension τ at either ends. The membrane is assumed to be composed of two layers, and a certain concentration of polymer lipids is desolved in each layer. The polymer lipids can freely diffuse within each layer, but they cannot move between layers. The concentrations of the polymer lipids in each layer are denoted by η and ζ. The shape of the membrane (string) is described by the tangential angle $\varphi(s)$ at the point s which is the distance measured along the membrane from one end. The free energy of the membrane is expressed by the following equation, using the Helfrich free energy [18]:

$$F=\int_0^L\left\{\frac{\kappa}{2}\left(\frac{\partial\varphi}{\partial s}\right)^2+\frac{D}{2}\left(\frac{\partial\eta}{\partial s}\right)^2+\frac{D}{2}\left(\frac{\partial\zeta}{\partial s}\right)^2 -\Lambda(\zeta-\eta)\frac{\partial\varphi}{\partial s}+h(\eta)+h(\zeta)\right\}ds. \tag{1}$$

Here κ is the bending modulus, and the first term expresses the bending energy. The second and third terms are the energies arising from the gradients of the polymer lipid concentrations. The coupling between the curvature and the concentrations of polymer lipids is given by the fourth term [9]. This coupling term exists because the long polymer parts of the polymer lipids ''prefer'' a curvature, because a larger spacing is entropically favorable for the long polymers [19]. The fifth and sixth terms represent the repulsive interactions between the long polymers in each layer [20,21]. This interaction prevents the concentration of polymer lipids from being too high in any curved region, where polymer lipids tend to gather. There are additional conditions regarding the conservation of polymer lipids as well as a boundary condition which defines the direction of the membrane (string). These conditions are written as

$$\int_0^L \eta(s)ds = \int_0^L \zeta(s)ds = \eta_0 L, \tag{2}$$

$$\int_0^L \sin\varphi(s)ds = 0, \tag{3}$$

where η_0 is the average concentration of polymer lipids in each layer. If we assume a periodic boundary condition, $\varphi(L+s)=\varphi(s)$, then the boundary condition in Eq. (3) is automatically satisfied, and the free energy of the membrane with tension τ is given by

$$H = F - \tau \int_0^L \cos\varphi \; ds. \tag{4}$$

There are additional conditions on the polymer lipid concentrations $\eta(s)$ and $\zeta(s)$ which must be taken into account when the average concentration η_0 is small. Since each polymer lipid has a tendency to move to a region of higher curvature as a result of the interaction between the lipid and the curvature, the concentrations of polymer lipids in low curvature regions decrease and become nearly zero in some cases. However, the concentration cannot be negative. Thus we must add the following conditions to obtain the minimum value of the free energy H:

$$\eta(s) \geqslant 0 \quad \text{and} \quad \zeta(s) \geqslant 0. \tag{5}$$

III. LINEAR STABILITY AND THERMAL FLUCTUATION

In the formula of the free energy [Eq. (4)], the parameter Λ represents the strength of the coupling between the curvature of the membrane and the polymer lipid concentration. When Λ is larger than a certain value, polymer lipids move to regions of larger curvature, and the curvatures of these regions grow more. This is the curvature instability mentioned above. In this section we determine the parameter regions in which undulation of the membrane due to the curvature instability is observed. This region changes due to the presence of thermal fluctuations (existing when the temperature $T>0$).

As a first step, we investigate the case without thermal fluctuations ($T=0$). In this case, using the free energy [Eq. (4)], the linear stability of a flat membrane determines the parameter region of the curvature instability for η_0 and τ. A flat membrane is defined by $\varphi=0$, $\eta=\eta_0$, and $\zeta=\eta_0$. Deviations from a flat state are represented by the following Fourier series:

$$\varphi = \sum_{m=1}^{\infty} \{\varphi_{sm}\sin(k_m s) + \varphi_{cm}\cos(k_m s)\}, \tag{6}$$

$$\eta = \eta_0 + \sum_{m=1}^{\infty} \{\eta_{sm}\sin(k_m s) + \eta_{cm}\cos(k_m s)\}, \tag{7}$$

$$\zeta = \eta_0 + \sum_{m=1}^{\infty} \{\zeta_{sm}\sin(k_m s) + \zeta_{cm}\cos(k_m s)\}. \tag{8}$$

After substituting Eqs. (6)–(8) into Eq. (4), and including only up to second order terms in the Fourier expansion of each coefficient, we obtain the free energy as

$$\begin{aligned} H = \frac{L}{2}\sum_{m=1}^{\infty} \Bigg\{ & \left(\frac{\kappa}{2} k_m^2 (\varphi_{sm}^2 + \varphi_{cm}^2) \right) + \frac{1}{2}[D k_m^2 + h''(\eta_c)] \\ & \times (\eta_{sm}^2 + \eta_{cm}^2 + \zeta_{sm}^2 + \zeta_{cm}^2) + \Lambda k_m (\zeta_{sm} - \eta_{sm})\varphi_{cm} \\ & - \Lambda k_m (\zeta_{cm} - \eta_{cm})\varphi_{sm} + \frac{\tau}{2}(\varphi_{sm}^2 + \varphi_{cm}^2) \Bigg\}. \end{aligned} \tag{9}$$

The stability of mode m is determined by the eigenvalues obtained from the following eigenvalue equation:

$$\begin{aligned} \lambda^2 - \lambda\{(\kappa + D)k_m^2 + h''(\eta_0) + \tau\} + (\kappa k_m^2 + \tau)(D k_m^2 + h''(\eta_0)) \\ - 2\Lambda^2 k_m^2 = 0. \end{aligned} \tag{10}$$

If one of these eigenvalues is negative, this mode is unstable. The mode m is unstable when the tension τ satisfies the relation

$$\tau < -\kappa k_m^2 + \frac{2\Lambda^2 k_m^2}{D k_m^2 + h''(\eta_0)}. \tag{11}$$

Maximizing the right-hand side of Eq. (11) with respect to the wave number k_m, we obtain the unstable region for parameters τ and η_0 as

$$\tau < \frac{\Lambda^2}{D}\left(\sqrt{2} - \sqrt{\frac{\kappa h''(\eta_0)}{\Lambda^2}} \right)^2. \tag{12}$$

The mode which becomes unstable first as the tension τ is decreased from a large value is written as

$$k_*^2 = \frac{\Lambda^2}{D\kappa}\sqrt{\frac{\kappa h''(\eta_0)}{\Lambda^2}}\left(\sqrt{2} - \sqrt{\frac{\kappa h''(\eta_0)}{\Lambda^2}} \right), \tag{13}$$

where $\Lambda^2/\kappa h''(\eta_0) > \frac{1}{2}$ must be satisfied.

As the next step, we consider the effect of thermal fluctuations on the curvature instability. When the concentration of polymer lipids η_0 is extremely small and the temperature

T is finite, thermal fluctuations of polymer concentrations are enhanced, and a fluctuating flat membrane is observed even if there are unstable modes in the system, because amplitudes corresponding to unstable modes are small, and the localization of polymer lipids is not favorable entropically. On the other hand, when the concentration of polymer lipids η_0 is not small, the entropy effect is less important, and the amplitudes of unstable modes increase. In these cases, undulations of membranes are realized in some parameter regions. We discuss the thermal fluctuations of flat membranes in thermodynamic equilibrium. The partition function Z is defined as

$$Z=\sum \exp(-\beta H), \tag{14}$$

where the summation is taken over all possible states, and we use the measure

$$\sum =\prod_m \int d\varphi_{sm}\int d\varphi_{cm}\int d\eta_{sm}\int d\eta_{cm}\int d\zeta_{sm}\int d\zeta_{cm}. \tag{15}$$

Since the conditions $\eta(s)\geqslant 0$ and $\zeta(s)\geqslant 0$ must be satisfied, as an approximation, we use the measure

$$\int_{-\eta_0}^{\eta_0} d\eta_{sm}\int_{-\eta_0}^{\eta_0} d\eta_{cm}\int_{-\eta_0}^{\eta_0} d\zeta_{sm}\int_{-\eta_0}^{\eta_0} d\zeta_{cm}. \tag{16}$$

The part of the partition function Z associated with φ_{cm} is written as

$$Z_{cm}=\int d\varphi_{cm}\int_{-\eta_0}^{\eta_0} d\eta_{sm}\int_{-\eta_0}^{\eta_0} d\zeta_{sm}\exp(-\beta H_{cm}), \tag{17}$$

where H_{cm} is the energy associated with the mth mode φ_{cm} and $\beta=1/k_BT$ (k_B is the Boltzmann constant and T is the temperature). This partition function Z_{cm} is expressed as

$$Z_{cm}=\int_{-\infty}^{\infty} d\varphi\ \exp\left(-\frac{L}{2}B_m\varphi^2\right)\times\left\{\int_{-\eta_0}^{\eta_0} d\eta\ \exp\left[-\frac{L}{2}A_m\left(\eta^2-\frac{\Lambda k_m}{A_m}\varphi\eta\right)\right]\right\}^2, \tag{18}$$

where A_m and B_m are defined by $A_m=[Dk_m^2+h''(\eta_0)]/2$, and and $B_m=(\kappa k_m^2+\tau)/2$. In Eq. (18), β is absorbed into each parameter τ, Λ, κ, D and h''. The partition function Z_{cm} is modified as

$$Z_{cm}=\int_0^{\infty} d\varphi\ \exp\left[-\frac{L}{2}\left(B_m-\frac{\Lambda^2k_m^2}{2A_m}\right)\varphi^2\right]\frac{2}{LA_m}T_m^2, \tag{19}$$

where T_m is defined by

$$T_m=\int_{-\sqrt{LA_m/2}[\eta_0-(\Lambda k_m/2A_m)|\varphi|]}^{\sqrt{LA_m/2}[\eta_0-(\Lambda k_m/2A_m)|\varphi|]} dx\ \exp(-x^2). \tag{20}$$

In the case that $\sqrt{LA_m/2}\,\eta_0\gg 1$ is satisfied, T_m is approximated by $T_m\simeq\sqrt{\pi}$ if $0\leqslant\varphi\leqslant(2A_m/\Lambda k_m)\eta_0$ or by $T_m\simeq 0$ if $(2A_m/\Lambda k_m)\eta_0<\varphi$. The partition function Z_{cm} can be estimated by

$$Z_{cm}\simeq\int_0^{(2A_m/\Lambda k_m)\eta_0} d\varphi\ \exp\left[-\frac{L}{2}\left(B_m-\frac{\Lambda^2k_m^2}{2A_m}\right)\varphi^2\right]\frac{2\pi}{LA_m}. \tag{21}$$

The average amplitude of fluctuations φ_{cm}^2 is calculated by the partition function Eq. (21) as

$$\langle\varphi_{cm}^2\rangle\simeq\frac{2}{L\left|B_m-\frac{\Lambda^2k_m^2}{2A_m}\right|}\frac{\int_0^{X_m}x^2\exp(-\alpha x^2)dx}{\int_0^{X_m}\exp(-\alpha x^2)dx}, \tag{22}$$

where X_m is defined by

$$X_m=\sqrt{\frac{L}{2}\left|B_m-\frac{\Lambda^2k_m^2}{2A_m}\right|}\frac{2A_m}{\Lambda k_m}\eta_0, \tag{23}$$

and α is the sign of $B_m-(\Lambda^2k_m^2/2A_m)$. When $B_m-(\Lambda^2k_m^2/2A_m)\geqslant 0$ and $X_m\gg 1$, the energy of the mth mode becomes

$$\frac{L}{2}\left(B_m-\frac{\Lambda^2k_m^2}{2A_m}\right)\langle\varphi_{cm}^2\rangle\simeq\frac{1}{2}. \tag{24}$$

This relation implies the equipartition of energy. When $B_m-(\Lambda^2k_m^2/2A_m)<0$ is satisfied, the mth mode is linearly unstable, and the energy of the unstable mode is estimated as

$$\frac{L}{2}\left(B_m-\frac{\Lambda^2k_m^2}{2A_m}\right)\langle\varphi_{cm}^2\rangle\simeq -X_m^2, \tag{25}$$

and the amplitude is written by

$$\langle\varphi_{cm}^2\rangle\simeq\left(\frac{2A_m}{\Lambda k_m}\right)^2. \tag{26}$$

In order to estimate the parameter region in which the curvature instability is observed, we assume the following three conditions. First, we assume that the undulation caused by unstable modes can be described by a single mode. This is the single-mode approximation [13]. Second, we assume that the amplitude of the unstable mode can be calculated from the partition function [Eq. (21)] when the instability is not strong. Third, as the observability condition of the unstable mode, we assume that the energy gained by the unstable mode is comparable to or larger than that of other thermally fluctuating modes. Then the number of thermally fluctuating modes Δm is $\Delta kL/2\pi$, where Δk is the length of the interval corresponding to stable wave numbers. Since the energy of one stable mode is 1/2 by equipartition of energy, the condition that the unstable mode can be observed is expressed by

$$X_m^2\geqslant\frac{L}{4\pi}\Delta k. \tag{27}$$

This relation can be written as

$$\left(\frac{\Lambda^2 k_m^2}{2A_m}-B_m\right)\left(\frac{2A_m}{\Lambda k_m}\eta_0\right)^2 \geqslant C, \tag{28}$$

where C is a certain constant. As the observable unstable mode, we choose the mode k_* given by Eq. (13). Then the observability condition of the unstable mode [Eq. (28)], is written as

$$\tau\frac{D}{\Lambda^2} \leqslant \left(\sqrt{2}-\sqrt{\frac{\kappa h''(\eta_0)}{\Lambda^2}}\right)\left\{\sqrt{2}-\sqrt{\frac{\kappa h''(\eta_0)}{\Lambda^2}} - k_B T\frac{D}{\Lambda^2}C\sqrt{\frac{\Lambda^2}{\kappa h''(\eta_0)}}\Big/\left(\sqrt{\frac{D}{\kappa}}\eta_0\right)^2\right\}, \tag{29}$$

where the temperature dependence of each parameter τ, Λ, κ, D, and h'' is explicitly represented. The observability condition [Eq. (29)] can be considered as a relation between the tension τ and the polymer lipids concentration η_0, and is depicted in Fig. 8 in Sec. V. This condition describes the results of Monte Carlo simulations quite well.

IV. COMPUTER SIMULATION

In this section, we give numerical results obtained by Monte Carlo simulation for the model defined in Sec. II. The model equations used for simulations can be simplified by the following rescaling:

$$g'=\frac{D}{\Lambda^2}G/L, \quad \tau'=\frac{D}{\Lambda^2}\tau, \quad s'=\sqrt{\frac{\Lambda^2}{D\kappa}}s,$$

$$k'=\sqrt{\frac{D\kappa}{\Lambda^2}}k, \quad \eta'=\sqrt{\frac{D}{\kappa}}\eta \quad \text{and} \quad \zeta'=\sqrt{\frac{D}{\kappa}}\zeta. \tag{30}$$

If we assume the energy expression

$$h(\eta)=\frac{a}{2}\eta^2+\frac{b}{4}\eta^4, \tag{31}$$

for the polymer lipid free energy, the total free energy of the membrane is described by

$$g'=\frac{1}{L}\int_0^L\left[\frac{1}{2}\left\{\left(\frac{\partial\varphi'}{\partial s'}\right)^2+\left(\frac{\partial\eta'}{\partial s'}\right)^2+\left(\frac{\partial\zeta'}{\partial s'}\right)^2\right\}-(\zeta'-\eta')\frac{\partial\varphi'}{\partial s'} + \frac{\kappa a}{\Lambda^2}\left(\frac{\eta'^2+\zeta'^2}{2}+\frac{\kappa b}{Da}\frac{\eta'^4+\zeta'^4}{4}\right)-\tau'\cos\varphi'\right]ds'. \tag{32}$$

In this expression, $\kappa a/\Lambda^2$ and $\kappa b/Da$ are two dimensionless parameters which characterize the system. The first parameter $\kappa a/\Lambda^2$ represents the strength of curvature instability, and the second parameter $\kappa b/Da$ determines the amplitude of $\varphi(s)$ and $\eta(s)$. For convenience, we omit the symbol $'$ on each variable in Eq. (32) from this point.

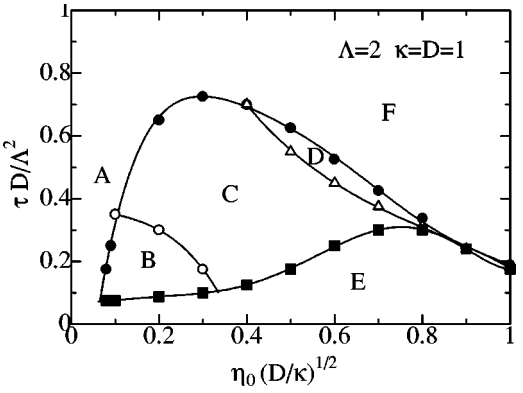

FIG. 2. Phase diagram obtained by Monte Carlo simulations for $\Lambda=2$ and $\kappa=D=a=b=1$. The rescaled tension $\tau D/\Lambda^2$ is plotted as a function of the rescaled polymer lipid concentration $\eta_0(D/\kappa)^{1/2}$. The regions from A to F correspond to different characteristic shapes of the membrane. A: Thermal fluctuations. B: Localized large deformations. C: Undulation over the entire membrane. D: Domain structures of undulation. E: Winding structures. F: Stable flat membrane. The boundaries between A and F and between A and E are not drawn in this phase diagram.

In order to minimize the free energy expressed by Eq. (32), we used the following Monte Carlo scheme. We divided the membrane (string) of length L into N segments represented by N points, and discretized the variables φ, η, and ζ at each point. To change φ, we chose two points and then changed the values φ at these points by small quantities so as to satisfy the boundary condition [Eq. (3)]. For η and ζ, we used Kawasaki dynamics [22], which consists of the exchange of small amounts of polymer lipids between two neighboring points. In order to perform finite-temperature simulations, we adopted the Metropolis method to determine whether the new state is accepted. The new values of φ, η, or ζ are accepted if the energy of the new state is smaller than that of the old one, i.e., ΔF is negative. If ΔF is positive, the new state is accepted with the probability $\exp(-\Delta F/k_B T)$. One Monte Carlo step is composed of N trials for each variable φ, η, and ζ. These Monte Carlo steps continue until the system is considered to be in equilibrium. In our simulations $N=256$, and the number of Monte Carlo steps is 10^5.

The results of the Monte Carlo simulations are summarized as follows. The parameters were fixed as $\kappa=D=a=b=100k_B T$ and $\Lambda^2/\kappa a=4$. Varying the average concentration η_0 and tension τ, we sought the equilibrium states and plotted them in a phase space (Fig. 2) defined by $\eta_0(D/\kappa)^{1/2}$ and $\tau D/\Lambda^2$. The following six characteristic shapes were observed.

(1) A thermally fluctuating flat membrane found in region A of Fig. 2 Slow thermal fluctuations are observed in this region, but regular undulation is not observed. As reflected by the power spectrum of φ, the amplitudes of unstable modes are not large, compared with those of thermally fluctuating modes. This fluctuating membrane appears when the average concentration η_0 of polymer lipids is very small. Since the concentration η_0 is small, the strength of unstable modes cannot develop, and thermal fluctuations dominate the system.

(2) Localized large deformations (Fig. 3) found in region

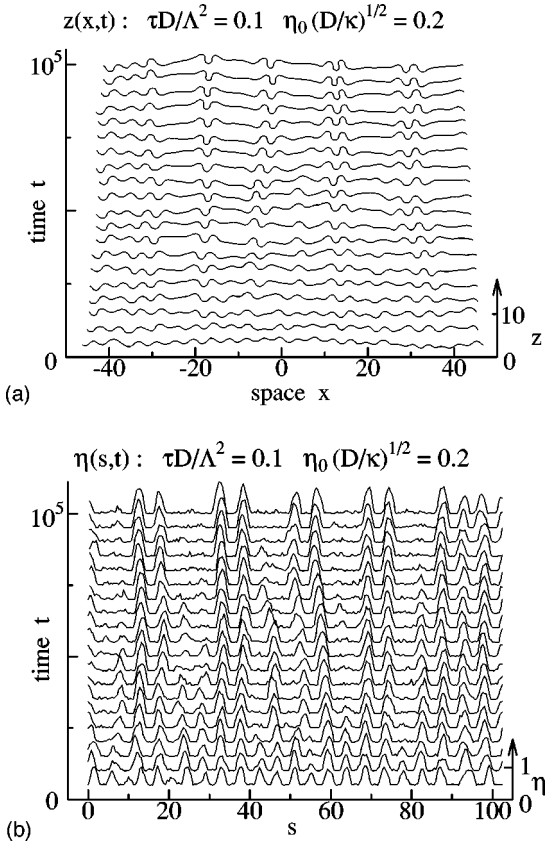

FIG. 3. The shape of large localized deformations in the membrane found in region *B* of Fig. 2. Here we have $\tau D/\Lambda^2=0.1$ and $\eta_0(D/\kappa)^{1/2}=0.2$. Other parameters are fixed as $\Lambda=2$ and $\kappa=D=a=b=1$. (a) The actual shape of the membrane is drawn as a function of time. The initial shape is flat, and the time interval between each shape drawn in the figure is 5000 Monte Carlo steps. (b) The development of the polymer lipid concentration $\eta(s)$ is shown. In the shape of the membrane displayed in (a), there are several localized undulations. Polymer lipids are also concentrated here. The concentration of polymer lipids in the nearly flat parts is almost zero.

B of Fig. 2. Here the concentrations of polymer lipids η and ζ are strongly localized in several areas, and large deformations of the membrane appear there. Both the concentration profile η and the shape of the membrane are shown in Fig. 3. When the concentration η_0 is relatively small, decreasing the tension τ from a large value, the flat membrane changes to exhibit weak undulation, and the undulation grows in several areas to become large localized deformations. Since the energy gain due to the coupling between the curvature and the polymer lipids is very large in the strongly deformed parts of the membrane, polymer lipids gather there from neighboring regions until no polymer lipids remain in these regions surrounding the localized deformations.

(3) The undulation of the entire membrane (Fig. 4) found in region *C* of Fig. 2. In this region, the regular undulation caused by the curvature instability extends over the entire area of the membrane, and does not fluctuate in time.

(4) Domain structures of undulating membranes (Fig. 5) found in region *D* of Fig. 2. The membrane is separated into several undulating domains which do not merge with each other in this region.

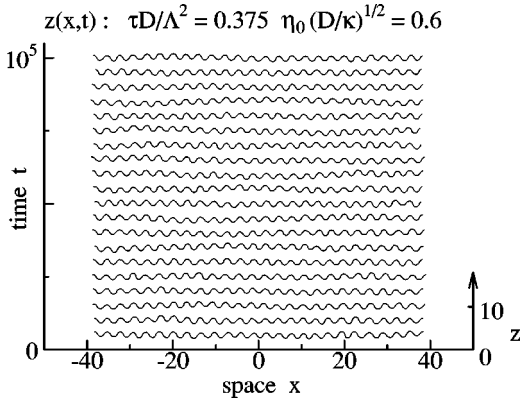

FIG. 4. Undulation extended in the entire area of the membrane found in region *C* of Fig. 2. The shapes of the membrane are drawn for times $5000i$, where $i=1,2,\ldots,20$. Here we have $\tau D/\Lambda^2=0.375$ and $\eta_0(D/\kappa)^{1/2}=0.6$. The membrane is uniformly undulating over the entire area.

(5) The winding membrane found in region *E* of Fig. 2. Here the amplitude of the undulation becomes very large, and some parts of the membrane contact or cross other parts. This situation is meaningless in our simulation scheme.

(6) The flat membrane with no fluctuation found in region *F* of Fig. 2. In this region, the flat membrane is not unstable with respect to any mode.

If we consider our one-membrane model as one kind of a mean-field model for multilamellar systems, the tension τ is understood as arising from the repulsive interactions between neighboring membranes in multilamellar systems, and τ becomes roughly proportional to d^{-x-2}, where d is the spacing between two membranes, and x is some positive number when the repulsive interaction is proportional to d^{-x}. Using this relation, we can redraw the phase diagram of Fig. 2 in the space defined by the concentration of polymer lipids η_0 and the average spacing d between neighboring membranes. The phase diagram so obtained has a structure quite similar to that in the phase diagram measured by experiments [5]. From this fact, we conjecture that a certain kind of strong

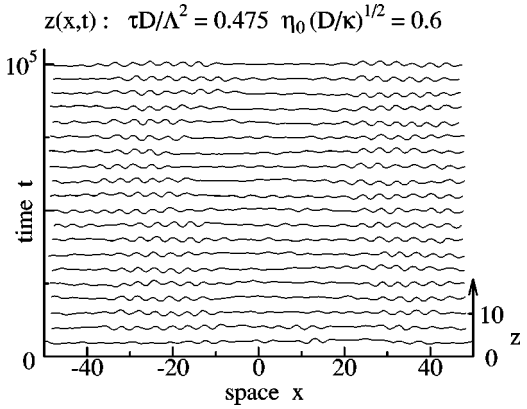

FIG. 5. Domain structures of undulation found in region *D* of Fig. 2. The rescaled parameters satisfy $\tau D/\Lambda^2=0.475$ and $\eta_0(D/\kappa)^{1/2}=0.6$. The shapes of the membranes are drawn at time intervals of 5000 time steps. The sequence of the membrane shapes shows that there are two different kinds of regions in the membrane. One is an almost flat region, and the other is an undulating region. The boundaries between the two regions move slowly.

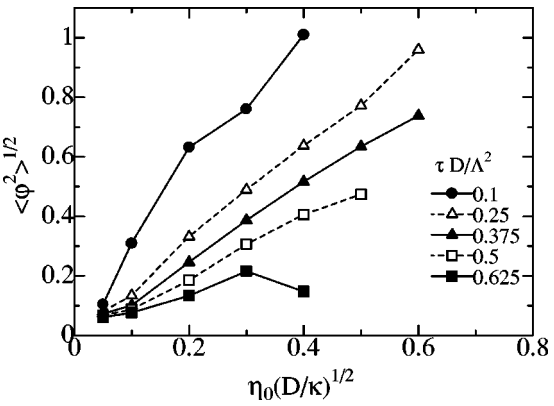

FIG. 6. Average amplitude of the tangential angle $\sqrt{\langle\varphi^2\rangle}$ calculated from the results of Monte Carlo simulations as a function of $\eta_0(D/\kappa)^{1/2}$. The data are plotted for cases in which the membrane is undulating or thermally fluctuating. Under constant tension, the amplitude grows with increasing η_0.

undulation in the one-membrane model corresponds to a state which contains many connected defects in multilamellar systems, and that weak undulation in the one-membrane system corresponds to the similar undulation in multilamellar systems.

In Fig. 6, the average amplitude of the tangential angle $\sqrt{\langle\varphi^2\rangle}$ is plotted. This quantity was calculated from the simulation results as a function of $\eta_0(D/\kappa)^{1/2}$ in the case when the membrane displays undulation. From the figure, the average amplitude $\sqrt{\langle\varphi^2\rangle}$ grows almost linearly, causing the concentration η_0 to increase under the constant tension $\tau D/\Lambda^2$. The growth rate of $\sqrt{\langle\varphi^2\rangle}$ becomes large when the tension $\tau D/\Lambda^2$ is small. This implies that large deformations take place by adding a small amount of polymer lipids when the tension is small.

We also calculated the η_0 dependence on the wave number k of undulation from the simulations. This result is given in Fig. 7. The characteristic wave number $k_{\max}$ was obtained numerically as the mode with the largest amplitude in the power spectrum of φ. Figure 7 shows that the wave number of the undulation does not depend strongly on either the concentration η_0 of polymer lipids or the tension τ, except in the case that the tension is small. The broken line in Fig. 7 represents the mode k_* given by Eq. (13), which first becomes unstable when the tension is decreased from a large value. We can say that the broken line gives the upper limit of the characteristic wave number $k_{\max}$ obtained through simulation and that the wave number of undulation $k_{\max}$ is nearly equal to k_*, given by Eq. (13).

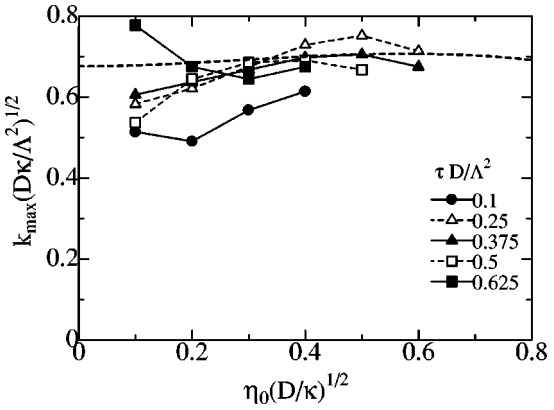

FIG. 7. Rescaled characteristic wave number $k_{\max}(D\kappa/\Lambda^2)^{1/2}$ as a function of the rescaled polymer lipid concentration $\eta_0(D/\kappa)^{1/2}$. The characteristic wave number $k_{\max}$ represents the strongest mode, with the maximum amplitude of φ, measured from the power spectrum for φ. When $\eta_0(D/\kappa)^{1/2}<0.2$, the membrane is thermally fluctuating. $k_{\max}$ does not depend strongly on η_0. Except for $\tau D/\Lambda^2=0.1$, definite τ dependence of $k_{\max}$ is not seen.

V. SINGLE-MODE APPROXIMATION

In this section we analyze a membrane possessing undulation using the single-mode approximation [13], which is the assumption that the shape of an undulating membrane caused by the curvature instability is approximately characterized by only one unstable mode. From the fact that the polymer lipids concentration η and ζ are both positive, we find that there are two kinds of solutions resulting from the single-mode approximation, depending on the polymer lipid concentration η_0 and the tension τ. When the concentration η_0 and the tension τ are near the critical line of the instability, the instability is weak, and the following type of solution (type A) can be assumed:

$$\varphi(s)=A\ \cos(ks), \tag{33}$$

$$\eta(s)=B\ \sin(ks)+\eta_0, \tag{34}$$

$$\zeta(s)=-B\ \sin(ks)+\eta_0. \tag{35}$$

Here A and B are the amplitudes of the tangential angle φ and the concentration η. This solution is valid only when

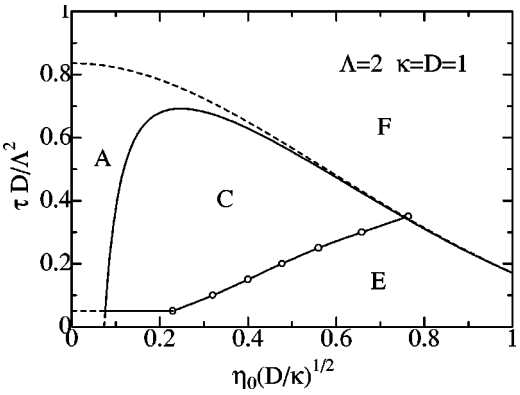

FIG. 8. Phase diagram calculated using linear stability analysis and the single-mode approximation. The rescaled tension $\tau D/\Lambda^2$ is plotted vs the rescaled polymer lipid concentration $\eta_0(D/\kappa)^{1/2}$. All parameters are the same as those in Fig. 2. The broken line is the critical line of instability given by Eq. (12), and the solid line is the theoretical estimate given by Eq. (29), which represents the condition that the amplitude of an unstable mode becomes larger than that of thermal fluctuations. We set the parameter C in Eq. (29) as $C=0.01/k_BT$. The line with circles represents the boundary on which the amplitude of φ becomes 1.42. Corresponding to the phase diagram shown in Fig. 2, characteristic shapes of the membrane are found in the regions A, C, E, and F. A: Thermal fluctuations. C: Undulation over the entire membrane. E: Winding structures. F: Stable, flat membrane.

$B<\eta_0$ is satisfied. Substituting Eqs. (33)–(35) into Eq. (32), the free energy is described as

$$g=\frac{1}{4}k^2A^2-kAB + \frac{1}{2}k^2B^2+\frac{1}{2\pi}\int_0^{2\pi}\left\{2\frac{D}{\Lambda^2}h\left(\sqrt{\frac{\kappa}{D}}(B\sin x+\eta_0)\right) - \tau\cos(A\ \cos x)\right\}dx. \tag{36}$$

The values of A, B, and k are determined to minimize the free energy [Eq. (36)].

In the case when the parameters η_0 and τ are far from the critical line of the instability, the instability becomes relatively strong. In this case, the concentration of polymer lipids becomes very large in regions of large curvature, and almost zero in other regions. Therefore, in these parameter regions, we can approximate the solution by the following piecewise-continuous solution (type B):

$$\varphi(s)=A\ \cos(ks), \tag{37}$$

$$\eta(s)=\max[B\ \sin(ks)+\eta_1,0], \tag{38}$$

$$\zeta(s)=\max[-B\ \sin(ks)+\eta_1,0], \tag{39}$$

where max[x,y] represents the larger of the values x and y. This solution is supplemented by the conservation of polymer lipid concentration, expressed by

$$\eta_0=\langle\eta(s)\rangle=\frac{1}{L}\int_0^L\eta(s)ds. \tag{40}$$

Substituting Eq. (38) into Eq. (40), this conservation is rewritten as

$$\tan\left(\frac{\pi}{2}y\right)-\frac{\pi}{2}y=\pi\left(\frac{\eta_0}{\eta_1}-1\right), \tag{41}$$

where y is introduced by $y=1-2ks_1/\pi$, and s_1 satisfies $B\ \sin(ks_1)=\eta_1$. Using the variable y, this definition for s_1 is equivalent to

$$\cos\left(\frac{\pi}{2}y\right)=\frac{\eta_1}{B}. \tag{42}$$

Substituting the assumed solution [Eqs. (37)–(39)] into Eq. (32), the free energy is calculated as

$$g=\frac{1}{4}k^2A^2+\left\{-kAB+\frac{1}{2}k^2B^2\right\}\left\{1-\frac{y}{2}+\frac{\sin(\pi y)}{2\pi}\right\} + \frac{1}{2\pi}\int_{-\pi/2}^{\pi/2}\frac{D}{\Lambda^2}h\left(\sqrt{\frac{\kappa}{D}}(B\sin x+\eta_1)\right)dx - \frac{1}{2\pi}\int_0^{(\pi/2)y}\frac{D}{\Lambda^2}h\left(\sqrt{\frac{\kappa}{D}}(-B\cos x+\eta_1)\right)dx$$

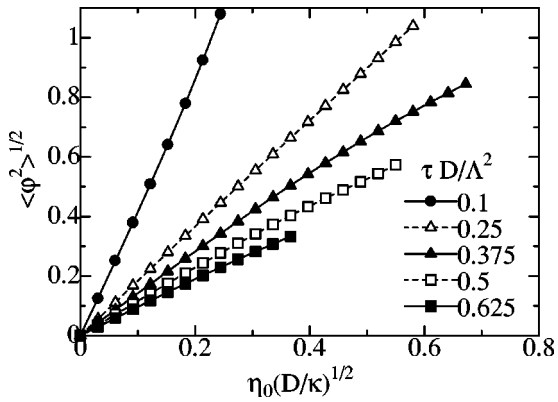

FIG. 9. Average amplitude of the tangential angle $\sqrt{\langle\varphi^2\rangle}$ as a function of the rescaled concentration $\eta_0(D/\kappa)^{1/2}$, calculated using the single-mode approximation of type B. Nearly linear growth is seen when η_0 is small. This figure should be compared with Fig. 6.

$$-\frac{2\tau}{\pi}\int_0^{\pi/2}\cos(A\ \cos x)dx. \tag{43}$$

When η_0 and τ are given, A, B, k, and η_1 are determined by minimizing the energy [Eq. (43)], with respect to A, B, and k under the conditions represented by Eqs. (41) and (42), which define the functions $\eta_1(B,\eta_0)$ and $y(B,\eta_0)$.

From numerical calculations for solutions of types A and B, we find that type A solutions exist only quite near the critical line of instability, and that almost all solutions in other regions of instability are of type B. In Fig. 8, we draw the parameter regions (regions A and C in Fig. 8) in which the solutions of types A and B exist. These regions are also limited to those points for which $\varphi<1.42$. The boundary representing the limit of the existence of stable solutions (type A or B) coincides with the critical line of the curvature instability, given by Eq. (12). The line satisfying $A=1.42$ corresponds to the boundary at which the undulation solution changes to a winding solution (for which some parts of the membrane touch other parts), as determined by the shapes of strings obtained through Monte Carlo simulations. (Parameters values here are $\Lambda=2,\kappa=D=a=b=1$, and $1/k_BT=100$.) From these observations, we can conclude that the following two conditions determine the parameter region in which undulating membranes exist: (1) The amplitude of the unstable mode is larger than the amplitude characterizing thermal fluctuations. (2) A solution found from the single-mode approximation exists, and the amplitude of the tangential angle φ is smaller than a certain value (in this case $|\varphi|<1.42$). Comparing Figs. 2 and 8, the region (denoted as C in Fig. 8) which satisfies these two conditions corresponds well with the regions (denoted as B, C, and D in Fig. 2) in which undulation of membranes are found in Monte Carlo simulations.

In Fig. 9, we show the relation between the amplitudes $\sqrt{\langle\varphi^2\rangle}$ of tangential angles for solutions (type B) and the polymer lipid concentration $\eta_0(D/\kappa)^{1/2}$. As η_0 is increased with constant tension $\tau D/\Lambda^2$, $\sqrt{\langle\varphi^2\rangle}$ increases monotonically, and almost linearly when $\eta_0(D/\kappa)^{1/2}$ is small. Figure 9 corresponds to Fig. 6, which was obtained from the results of Monte Carlo simulations. Since the solution obtained in the single-mode approximation does not include effects of ther-

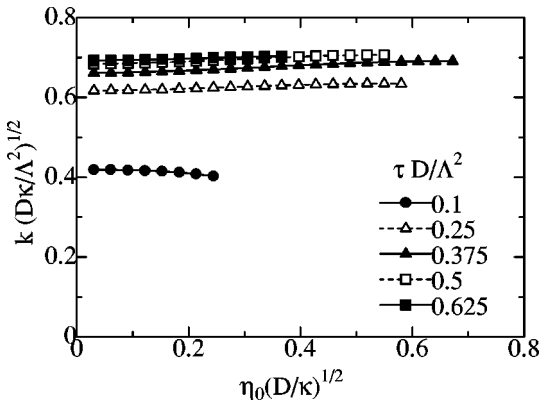

FIG. 10. Rescaled wave number $k(D\kappa/\Lambda^2)^{1/2}$ as a function of the rescaled polymer lipid concentration $\eta_0(D/\kappa)^{1/2}$, obtained using the single-mode approximation of type B. The wave number is nearly independent of the concentration η_0, but a slight τ dependence is found, especially for small τ. This figure should be compared with Fig. 7.

mal fluctuation and localized structures which are observed in Monte Carlo simulations, the average amplitudes $\sqrt{\langle\varphi^2\rangle}$ in the figures do not correspond precisely, but the global tendencies are very similar.

In order to characterize the undulation, we also calculated the wave number k of the solutions (type B) obtained in the single-mode approximation, and plotted them with respect to the polymer lipid concentration η_0 in Fig. 10. From this figure, we find that the wave number k is almost independent of the concentration η_0, and that the τ dependence is also small when τ is larger than a certain value. This behavior was also observed in the Monte Carlo simulations (see Fig. 7). In the Monte Carlo simulations, the tension τ dependence seems smaller than that seen in the single-mode approximation. According to the good correspondence between Figs. 8, 9, and 10 and Figs. 2, 6, and 7, we can conclude that the single-mode approximation is quite adequate in describing the undulation of membranes.

VI. CONCLUSION

In this paper, we studied the shape transformations of a one-lipid membrane system with lateral tension and polymer lipids as a kind of approximation of multilamellar systems. Using Monte Carlo simulations, we found several characteristic shapes of the membrane, including localized large deformations and regular undulations. We used the single-mode approximation to analyze the undulations of the membrane, and found that the results obtained by Monte Carlo simulation can be explained well with the theory derived from this approximation. The region in which the undulation is observed in the membrane is restricted by three conditions: (1) the curvature instability exists, (2) the instability is stronger than thermal fluctuations, and (3) the instability is not so strong that some parts of the membrane touch other parts. The phase diagram in the space of the polymer lipid concentration and the tension determined by the simulations has a structure quite similar to that observed in experiments on ''biogels'' [5]. This result indicates that defects found in multilamellar systems correspond to certain kinds of strong undulations of a single membrane with tension. Since the undulations occur as a result of the curvature instability, we conjecture that the complicated defect structures in ''biogels'' [6] are also caused by the curvature instability which results from the interaction between the polymer lipids and the curvature of the membranes.

In our model, when the concentration of polymer lipids is quite small, thermal fluctuations dominate, and undulation cannot be observed. This fact corresponds well to the fact that only a small number of defects can be observed in ''biogels'' when the polymer lipid concentration is small. These thermal defects can be understood as an entropy effect discussed in a previous paper [7].

Since our model is a one-membrane system, we cannot discuss defect structures found in multilamellar systems, but we can conclude that the three conditions mentioned above—curvature instability, fluctuations and vesiculation—play important roles in defect formation in multimembrane systems. As shown by direct observations [6], the connectivity between vesicular defects is considered to be the cause of gel viscosity in ''biogels.'' To observe the defect structure in multilamellar systems is quite important. Such work is now in progress using Monte Carlo simulations, where defect structures similar to those observed in experiments have been found under suitable conditions [23].

[1] *Micelles, Membranes, Microemulsions, and Monolayers*, edited by W. M. Gelbart, A. Ben-Shaul, and D. Roux (Springer, New York, 1993).
[2] M. Goulian, R. Bruinsma, and P. Pincus, Europhys. Lett. **22**, 145 (1993).
[3] R. Netz and P. Pincus, Phys. Rev. E **52**, 4114 (1995).
[4] P. Sens, M. S. Turner, and P. Pincus, Phys. Rev. E **55**, 4394 (1997).
[5] H. E. Warriner, S. H. Idziak, N. L. Slack, P. Davidson, and C. R. Safinya, Science **271**, 969 (1996).
[6] S. L. Kellar, H. E. Warriner, C. R. Safinya, and J. A. Zasadzinski, Phys. Rev. Lett. **78**, 4781 (1997).
[7] T. Kohyama, Physica A **28**, 323 (1998).
[8] P. G. de Gennes, *Scaling Concepts in Polymer Physics* (Cornell University Press, Ithaca, NY, 1979).
[9] S. Leibler, J. Phys. (France) **47**, 507 (1986).
[10] S. Leibler and D. Andelman, J. Phys. (France) **48**, 2013 (1987).
[11] D. Andelman, T. Kawakatsu, and K. Kawasaki, Europhys. Lett. **19**, 57 (1992).
[12] T. Kawakatsu, D. Andelman, K. Kawasaki, and T. Taniguchi, J. Phys. II **3**, 971 (1993).
[13] T. Taniguchi, K. Kawasaki, D. Andelman, and T. Kawakatsu, J. Phys. II **4**, 1333 (1994).
[14] *Monte Carlo Methods in Statistical Physics*, edited by K. Binder (Springer, New York, 1986).

[15] W. Helfrich, Z. Naturforsch. A **33a**, 305 (1978).
[16] C. R. Safinya *et al.*, Phys. Rev. Lett. **57**, 2718 (1986).
[17] C. R. Safinya, E. B. Sirota, D. Roux, and G. S. Smith, Phys. Rev. Lett. **62**, 1134 (1989).
[18] W. Helfrich, Z. Naturforsch. C **28**, 693 (1973).
[19] C. Hiergeist and R. Lipowsky, J. Phys. II **6**, 1465 (1996).
[20] S. A. Safran, P. Pincus, and D. Andelman, Science **248**, 354 (1990).
[21] S. A. Safran, P. A. Pincus, D. Andelman, and F. C. MacKintosh, Phys. Rev. A **43**, 1071 (1991).
[22] K. Kawasaki, in *Phase Transitions and Critical Phenomena* edited by C. Domb and M. S. Green (Academic Press, 1972), Vol. 2, p. 443.
[23] T. Kohyama (unpublished).